

TABLE IV: Experiment Settings of XJTU-SES (one cycle).

| Step | Time | SA Setting | LOAD Setting | Energy System Working Mode | Spacecraft Scenario |
|------|-----------|-----------------|--------------|----------------------------|-----------------------------------------------------------------------|
| 1 | 0-10 min | normal | non-loaded | charge | sunlit area, sun orientation mode, no task |
| 2 | 10-25 min | normal | 5V*2.9A | shunt | sunlit area, sun orientation mode, non-orientational load task I |
| 3 | 25-35 min | normal | non-loaded | charge | sunlit area, sun orientation mode, no task |
| 4 | 35-50 min | low irradiance | 12V*2.4A | joint | sunlit area, ground orientation mode, ground orientation task II |
| 5 | 50-60 min | normal | non-loaded | charge | sunlit area, sun orientation mode, no task |
| 6 | 60-70 min | zero irradiance | non-loaded | leisure | shadow area, ground orientation mode, no task |
| 7 | 70-85 min | zero irradiance | 5V*2.9A | discharge | shadow area, ground orientation mode, non-orientational load task III |
| 8 | 85-95 min | zero irradiance | non-loaded | leisure | shadow area, ground orientation mode, no task |
| 9 | | | | | Back to Step 1 ... |

'charge' refers to the situation where SA only charges BAT without any load, 'shunt' refers to the situation where SA provides energy for both LOAD and BAT, 'joint' refers to the situation where SA and BAT provide energy for LOAD simultaneously, 'leisure' refers to the situation where there is no load and BAT is not charging, and 'discharge' refers to the situation where BAT only supplies energy to LOAD.

Under normal circumstances, the attitude and orbit control of a spacecraft ensures its orientation towards the sun to maximize the energy generated by the SA. However, when performing tasks such as imaging the ground targets, the spacecraft has to switch to a ground-oriented mode.

APPENDIX A MAXIMAL INFORMATION COEFFICIENT (MIC)

Options of nonlinear correlation measurement include methods based on Granger causality analysis and methods based on information-theoretic causal analysis. The former can only provide qualitative analysis results, and is prone to generating spurious causal phenomena for high-dimensional time series. Among the methods based on information-theoretic causal analysis, a mature and representative method is the Maximal Information Coefficient (MIC) [17]. Specifically, for two series set $A = \{a_i \mid i = 1, \dots, T\}$ and $B = \{b_i \mid i = 1, \dots, T\}$, the T is the length of these series. The calculation of MIC is based on the mutual information MI, which is defined as:

$$\text{MI}(A, B) = \sum_{A, B} p(a, b) \log \frac{p(a, b)}{p(a)p(b)}, \quad (10)$$

where the $p(a, b)$ is the joint probability density. $p(a)$ and $p(b)$ are the marginal distributions of $p(a, b)$. Then, the MIC values can be given by:

$$\text{MIC}(A, B) = \max_{|A||B| < h(T)} \frac{\text{MI}(A; B)}{\log \min \{|A|, |B|\}}, \quad (11)$$

In order to reduce the consumption of computing resources, we limit $|A| \times |B| < h(T)$ and $h(T) = T^{0.6}$. In general, MIC works well in practice when $h(T) = T^{0.6}$.

APPENDIX B EXPERIMENT SETTING

To fully reflect the working conditions of the energy system under various conditions, our experimental settings are shown in Table IV. This also simulates a complete operational cycle of a spacecraft. This dataset mainly focuses on the energy system of spacecraft, and can also provide reference for the research of ground photovoltaic equipment.

APPENDIX C SENSORS AND SIGNALS

Our open-source dataset is named XJTU-SES, which contains three sub-datasets with sampling frequencies of 1Hz, 0.5Hz, and 0.1Hz, respectively. And the data length of each

sub-dataset is greater than 20000. The details of the sensors are shown in Table V, which includes 33 sensors. This dataset is a forecasting dataset similar to ETTh1, with a specific focus on individual photovoltaic energy systems. It can be utilized for researches related to predictive maintenance and energy control and allocation. Currently, there are relatively abundant grid-level IES dataset resources, especially in smart grids field. However, there are very few public dataset resources for single photovoltaic devices, especially for spacecraft, mainly due to the difficulty of data acquisition and the principle of confidentiality. Nevertheless, given the significant economic value and potential losses incurred by these devices upon failure, predictive maintenance are essential. Consequently, we have released this dataset for contributing to the research about unit-level photovoltaic energy systems.

APPENDIX D VISUALIZATION OF SYNTHETIC DATASET EXPERIMENT RESULTS

The visualization results of the experiments on the synthetic datasets are shown in Fig. 8.

APPENDIX E COMPLETE VISUALIZATION OF XJTU-SES DATASET EXPERIMENT RESULTS

To demonstrate the deployment effect of the proposed method in practical scenarios for predictive maintenance, and to further showcase its advantages through comparison, we set up a 33-channels to 33-channels forecasting task on the XJTU-SES dataset. We set up three sets of control experiments: IES-STGNN with KoopmanGNN, IES-STGNN without KoopmanGNN (only TCN), and IES-STGNN replacing KoopmanGNN with SGC. They represent our new spatial information fusion paradigm, no spatial information fusion, and traditional spatial information fusion paradigm, respectively. We chose SGC because it is a relatively advanced graph convolution method and has shown good performance in Table II. Their visualization results are shown in Fig. 9. Through our analysis, we can draw the following conclusions:

TABLE V: Sensors and Signals of XJTU-SES

| Channels | Sensors | Channels | Sensors | Channels | Sensors |
|----------|---------------------|----------|------------------------|----------|------------------------|
| 1 | SA Voltage | 12 | BAT group1 Temperature | 23 | Task1 Load Current |
| 2 | SA Current | 13 | BAT group2 Voltage | 24 | Task1 Load Temperature |
| 3 | SA Power | 14 | BAT group2 Current | 25 | Task1 Load Power |
| 4 | Output Load Voltage | 15 | BAT group2 Temperature | 26 | Task2 Load Voltage |
| 5 | Output Load Current | 16 | BAT group3 Voltage | 27 | Task2 Load Current |
| 6 | Output Load Power | 17 | BAT group3 Current | 28 | Task2 Load Temperature |
| 7 | BCR Voltage | 18 | BAT group3 Temperature | 29 | Task2 Load Power |
| 8 | BCR Current | 19 | Bus Voltage | 30 | Task3 Load Voltage |
| 9 | BCR Power | 20 | Bus Current | 31 | Task3 Load Current |
| 10 | BAT group1 Voltage | 21 | Bus Power | 32 | Task3 Load Temperature |
| 11 | BAT group1 Current | 22 | Task1 Load Voltage | 33 | Task3 Load Power |

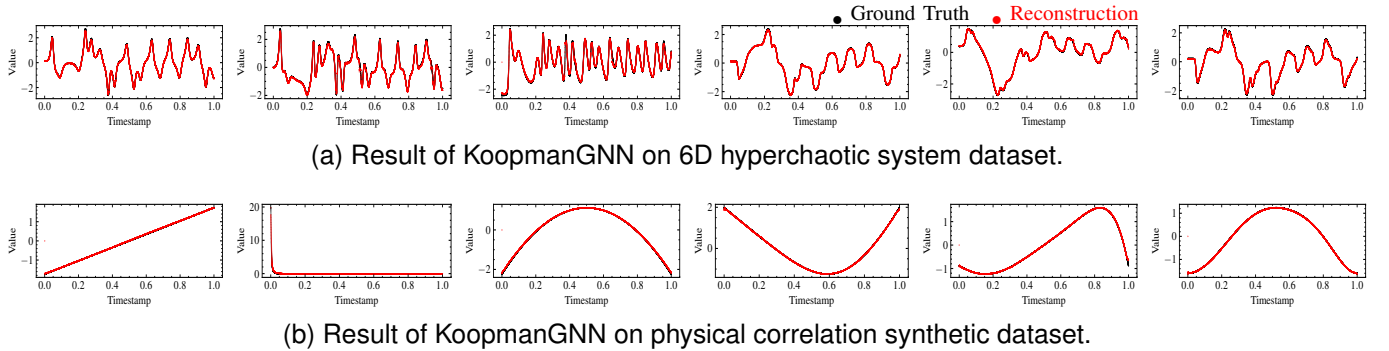


Fig. 8: Synthetic dataset experiment results. The MSE and MAE are computed as the averages across all channels.

- (1) As shown in Fig. 9b, TCN struggles to capture temporal patterns in datasets that temporal cyclic patterns are large-span and diverse changed, leading to unsatisfactory results. However, such scenarios, where a single cycle consists of approximately 2,500 timestamps or more, are common in the real world. For example, the mission types of spacecraft in operation are diverse, and their temporal pattern cycles are often proportional to the time it takes to orbit the Earth. Excessive downsampling might enhance TCN performance but would result in information loss, requiring larger datasets to provide sufficient temporal pattern information, and hinder rapid anomaly detection or fault diagnosis.
- (2) After introducing spatial information, as shown in Fig. 9a, the deployment of KoopmanGNN significantly enhances model performance. This is due to KoopmanGNN's ability to leverage the physical topological correlations among sensors in energy systems, effectively integrating and correcting the output information of TCN. This also demonstrates the effectiveness and necessity of KoopmanGNN.
- (3) Although spatial information is an important and indispensable source of information, within complex industrial systems like IES, the spatial information is complex and difficult to handle. As depicted in Fig. 9c, SGC fails to adequately capture the complex nonlinear correlations in the dataset, leading to over-smoothed forecasting results. The channels tend to become similar, which is a predictable outcome given the limitations of traditional methods in complex scenarios.
- (4) Therefore, we believe that spatial information is an important source of information in multi-sensor systems MTS tasks. It can be a breakthrough for further performance improvement.

However, the method for handling this information requires careful analysis of the inherent correlations. Techniques such as MIC and cosine similarity comparisons can serve as useful analysis tools. After analysis, if the spatial correlation information is linearity or simple nonlinearity, traditional graph convolution methods can be competent. But if it is complex nonlinearity, KoopmanGNN is a better option.

APPENDIX F SYNTHETIC DATASET DETAILS

To further discuss the advantages of KoopmanGNN, especially exploring what KoopmanGNN can uniquely capture, we created two synthetic datasets: a 6D hyperchaotic system dataset (as shown in (12)) and a physical correlation synthetic dataset (as shown in Table VI). Their common features are that they do not have periodic patterns, which means that accurate reconstruction can only be achieved by aggregating and processing the mutual correlations among other sensors, when self-connection is prohibited. Their differences lie in the nature of the correlations: the 6D hyperchaotic system dataset deliberately emphasizes differential operators, with each dependency incorporating a derivative term. The Physical correlation synthetic dataset intentionally selects complex nonlinear correlations devoid of differential operators, incorporating various physical laws and formulas.

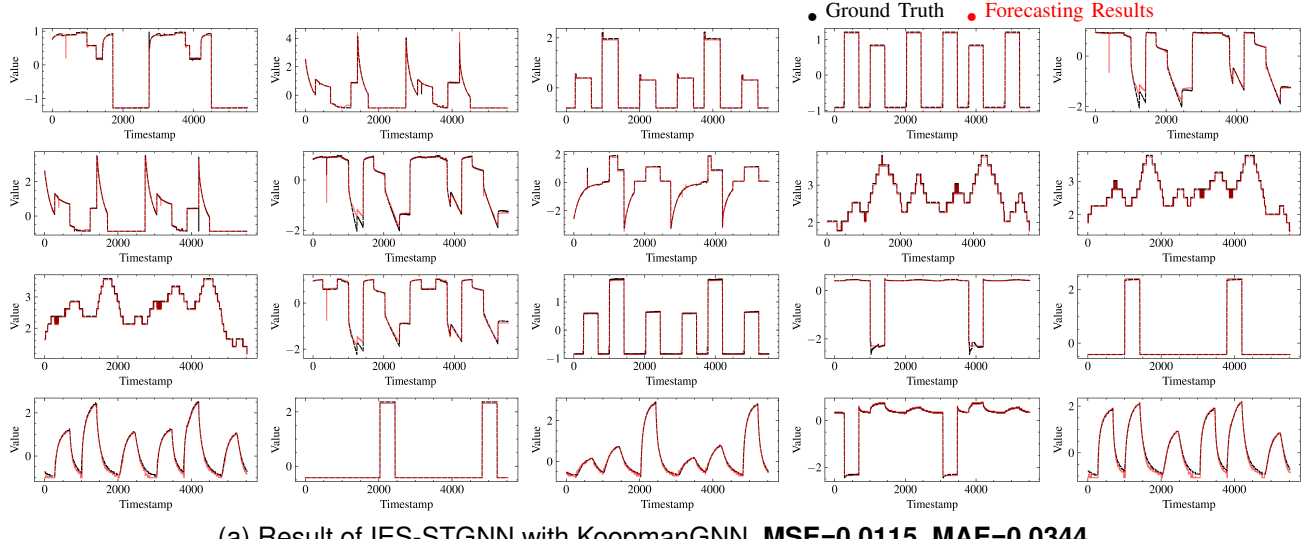
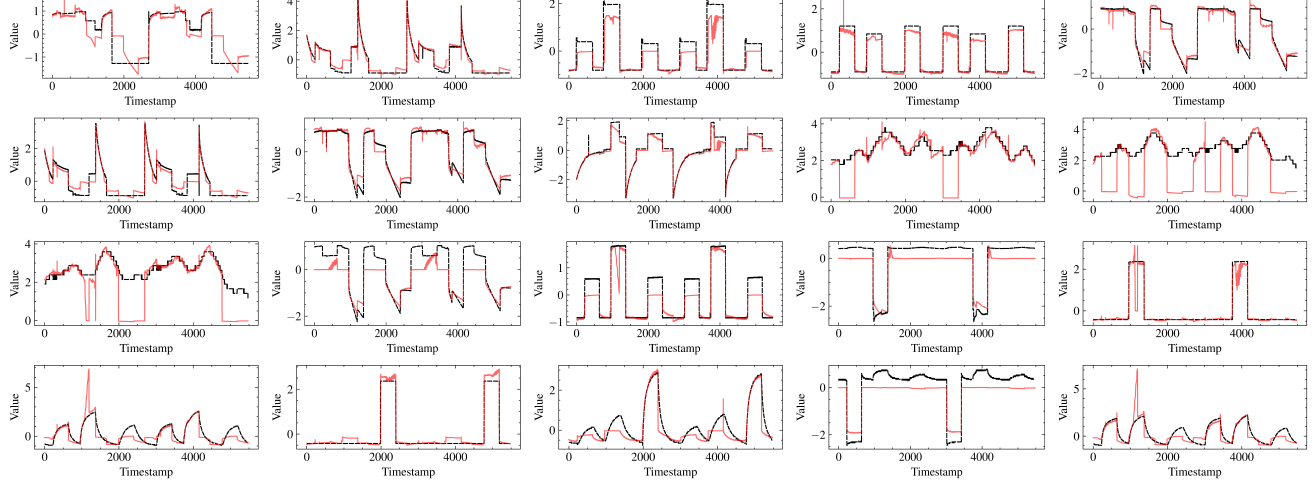
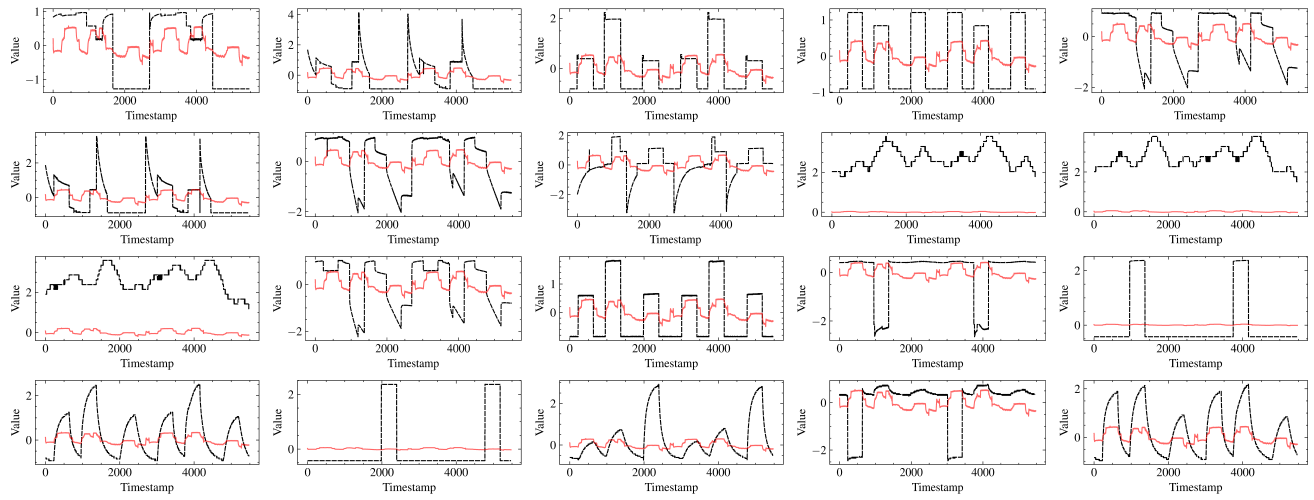
(a) Result of IES-STGNN with KoopmanGNN. **MSE=0.0115, MAE=0.0344**(b) Result of IES-STGNN w/o KoopmanGNN (only TCN). **MSE=0.301, MAE=0.285**(c) Result of IES-STGNN replace KoopmanGNN with SGC. **MSE=1.534, MAE=0.957**

Fig. 9: XJTU-SES Dataset Experiment Results. The MSE and MAE are computed as the averages across 20 channels. Due to the limited space, we only show some representative channels, which are SA Voltage, SA Current, Output Load Voltage, Output Load Current, BCR Voltage, BCR Current, BAT group1 Voltage, BAT group1 Current, BAT group1 Temperature, BAT group2 Temperature, BAT group3 Temperature, Bus Voltage, Bus Current, Task1 Load Voltage, Task1 Load Current, Task1 Load Temperature, Task2 Load Current, Task2 Load Temperature, Task3 Load Voltage, Task3 Load Temperature in sequence. The complete results of all channels can be found in <https://github.com/DiYi1999/KoopmanGNN>.

TABLE VI: Physical correlation synthetic dataset

| Channel | Correlation Type | Function |
|---------|------------------------------|----------------------------------------------------------------|
| 1 | Timestamp | t |
| 2 | Linear | $1 - t$ |
| 3 | Kinetic Energy Equation | $E = \frac{1}{2}mv^2$ |
| 4 | Law of Universal Gravitation | $F = G \frac{Mm}{r^2}$ |
| 5 | Coulomb's Law | $F = k \frac{q_1 q_2}{r^2}$ |
| 6 | Pythagorean Theorem | $c = \sqrt{a^2 + b^2}$ |
| 7 | Relativistic Velocity | $v = \frac{(v_1 - v_2)}{\left(1 - \frac{v_1 v_2}{c^2}\right)}$ |
| 8 | Lorentz Force | $F = qvB \sin(v, B)$ |
| 9 | Torque Force | $M = rF \sin(\theta)$ |
| 10 | Refraction Law | $\theta_1 = \sin^{-1} (n_2 \sin(\theta_2) \div n_1)$ |

$$\left\{ \begin{array}{l} \frac{dx}{dt} = a(y - x) + u, \\ \frac{dy}{dt} = cx - y - xz - v, \\ \frac{dz}{dt} = xy - bz, \\ \frac{du}{dt} = du - yz, \\ \frac{dv}{dt} = ry, \\ \frac{dw}{dt} = -ew + zu, \end{array} \right. \text{ s.t. } \left\{ \begin{array}{l} x(0) = 0.1, \quad a = 10, \\ y(0) = 0.1, \quad b = 2.6667, \\ z(0) = 0.1, \quad c = 28, \\ u(0) = 0.1, \quad d = -1, \\ v(0) = 0.1, \quad e = 10, \\ w(0) = 0.1, \quad r = 3. \end{array} \right. \quad (12)$$